CHINESE OPTICS LETTERS

Vol. 19, No. 11 | November 2021

Signal transmission of 4 GHz beyond the system bandwidth in UV-C LED communication based on temporal ghost imaging

Mengyin Jin (金梦茵)[1], Zeyuan Qian (钱泽渊)[1], Xinwei Chen (陈新伟)[1], Xugao Cui (崔旭高)[1], Ke Jiang (蒋 科)[2], Xiaojuan Sun (孙晓娟)[2], Dabing Li (黎大兵)[2*], and Pengfei Tian (田朋飞)[1**]

[1] Institute for Electric Light Sources, School of Information Science and Technology, and Academy of Engineering and Technology, Fudan University, Shanghai 200433, China

[2] State Key Laboratory of Luminescence and Applications, Changchun Institute of Optics, Fine Mechanics and Physics, Chinese Academy of Sciences, Changchun 130033, China

*Corresponding author: lidb@ciomp.ac.cn

**Corresponding author: pftian@fudan.edu.cn

Received March 5, 2021 | Accepted April 15, 2021 | Posted Online August 25, 2021

Due to the bandwidth limitation of the ultraviolet-C (UV-C) optical communication system and strong channel attenuation, it is difficult to transmit high-frequency signals. In this paper, the temporal ghost imaging (TGI) algorithm was first applied to the UV-C communication experimentally, and we realized the transmission of a 4 GHz signal through 95.34 MHz system bandwidth. The study indicates that the TGI algorithm can significantly improve the signal-to-noise ratio (SNR) compared with the on–off keying method. Our research provides a new approach for alleviating transmission frequency limitation due to poor SNR and insufficient hardware bandwidth.

Keywords: temporal ghost imaging; UV-C communication; ultra-high-frequency signal transmission.
DOI: 10.3788/COL202119.110602

1. Introduction

Ultraviolet (UV) communication has attracted the attention of many researchers in recent years, especially in the wavelength range of 200–280 nm, which is called UV-C[1–8]. This range of solar radiation can exist basically above the ozone layer, because it is almost absorbed by the ozone layer when it is incident on the earth's surface, and the intensity remaining below the ozone layer is negligible[9]. This allows UV-C to be used for satellite-to-satellite communications above the ozone layer without fearing wiretapping from the ground. Also, UV-C communication below the ozone layer can be affected barely by background noise.

However, it is considered that the UV-C light will be strongly scattered because of its short wavelength, which leads to serious light attenuation along the direction of light emission[10] and raises the possibility for non-line-of-sight (NLOS) communication. Long-range NLOS communication of 200 bps over 100 m has been achieved by using high light output power (LOP) UV-C light sources and high-sensitivity UV-C detectors such as a photomultiplier tube (PMT)[11–17]. To overcome the huge path loss (PL) caused by the long distance, one of the effective ways is to increase the LOP of the transmitter. However, the maximum permissible exposure of UV-C is specified due to the carcinogenicity[18]. Hence, many researchers are tentative to improve the long-range NLOS/line-of-sight (LOS) communication system performance by increasing the device bandwidth, optimizing coding and modulation methods, employing multiple input multiple output (MIMO), adopting spatial diversity, and so on[3,6,12,15–17,19–24]. Nevertheless, traditional LEDs are typically in millimeter sizes, and a larger size leads to larger capacitance and slower transistors' operating speed, which further inhibits bandwidth improvement[25]. The most recent modulation bandwidth record for large-size UV-C LEDs is 153 MHz[23]. Moreover, the bandwidths of commercial UV-enhanced detectors are generally limited to a few hundred megahertz (MHz)[26]. Therefore, optimizing the communication system performance based on large-size LEDs by increasing the modulation bandwidth of devices is challenging.

In recent years, temporal ghost imaging (TGI) has attracted the attention of many researchers as a modulation algorithm that can reduce the requirement of spatial and temporal resolution of detectors[27–29]. Sun *et al.* realized 3D single-pixel detector imaging, which is a very important application of spatial computational ghost imaging. Devaux *et al.* captured

non-repeatable time-domain signals without synchronization by the spatial computational ghost imaging system and realized the combination of spatial domain and time domain. Xu *et al.* conducted an experimental study of temporal computational ghost imaging, proving that TGI can lower the time resolution requirement of the detector. Relevant researches show that TGI can not only reduce the spatial or temporal resolution requirement of the detectors but also exhibit excellent anti-noise performance, improving the signal-to-noise ratio (SNR) of the system[28–33]. However, applying TGI to the UV-C communication system has not been reported yet.

In this paper, we introduce the TGI algorithm to the UV-C communication system through experiments for the first time, to the best of our knowledge. It was verified that a high-frequency temporal signal could be detected by a low-bandwidth detector based on TGI in a UV-C communication system. We realized the detection and reconstruction of a 4 GHz temporal signal when the system's bandwidth was less than 100 MHz. Meanwhile, it is proven that the TGI can realize the optimization of SNR. All of the results show that the TGI algorithm has great application potential in the UV-C communication field.

2. Methods and Experiments

In computational ghost imaging, modulation is achieved by multiplying the signal with a stack of random binary illuminated patterns in measurements. A second-order correlation between a stack of known illuminated patterns and the integration of the information received by the detector can retrieve the original signal[28]. Applying the aforementioned spatial modulation theory to the temporal domain, the repeatable temporal signal $T(t)$ can be modulated by a series of known temporal sequences $H_i(t)$ $(i = 1,2,\ldots,N)$, and then the low-bandwidth photodetector collects the integration of the product of the original signal and the modulation temporal sequences, which is represented as S_i[29]:

$$S_i = \sum_{t=1}^{N} H_i(t)T(t). \tag{1}$$

Here, we choose the Hadamard matrix as $H(t)$ whose dimension is the same as the length of the temporal signal, and each column of the Hadamard matrix is denoted as $H_i(t)$.

The second-order correlation between the received information and the modulation sequences is applied to retrieve the original signal[29]:

$$T'(t) = \langle S_i H_i(t)\rangle - \langle S_i\rangle\langle H_i(t)\rangle. \tag{2}$$

Here, $\langle\cdot\rangle$ denotes averaging of N measurements. The Hadamard matrix does not generate additional deviations theoretically compared with the random modulation matrix due to its good orthogonality, which makes the retrieved signal more proximate to the original signal[34]. In the presence of noise, the received information is composed of signals and noise, and the demodulation results correspond to the superposition of the correlation between signals and the modulation matrix and the correlation between noise and the modulation matrix. Because of the random statistical nature of noise and the lack of correlation between noise and the modulation matrix, the noise-related information can be alleviated, which makes the TGI algorithm robust to the noise[32].

Figures 1(a) and 1(b) show the schematic diagram of the experimental setup for the UV-C LED-based optical communication system and its picture, respectively. The original signal is 128-bit pseudo-random binary sequence (PRBS) code. The modulation of the original time signal was realized in MATLAB. After that, the transmitted signal was generated by an arbitrary waveform generator (AWG 710B, 4.2 GHz) and was loaded into the UV-C LED with a central wavelength of 277 nm as an AC component. The power supply provided a DC component to ensure that the LED worked at high emission power. The components of DC and AC were coupled through bias-tee (Mini-Circuits ZFBT-6GW+), and the superimposed electrical signal was used to drive the UV-C LED to transmit the optical signal. Then, the parameters were adjusted to ensure that the LED worked in the linear region. The transmitted optical signal passed through free space and was detected by the photodetector (Hamamatsu C12702-11, 100 MHz). At the receiving end, the received electrical signal was displayed on the oscilloscope in real-time, and, after being sampled, the LabVIEW offline program was applied to demodulate the sampled signal and evaluate the transmission performance. The transmitting frequency was adjusted on the AWG from 200 MHz to 4 GHz.

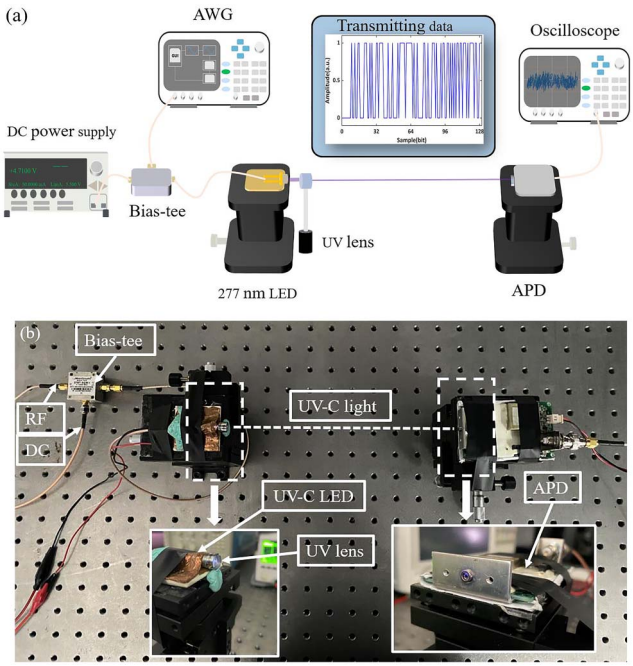

Fig. 1. (a) Schematic diagram for UV-C LED-based wireless optical communication system. (b) The photograph of the experimental setup.

3. Results and Discussion

The *I-V* characteristic of the UV-C LED is shown in Fig. 2(a). The best working point of the UV-C LED was determined to be 30 mA for the DC signal and 1.6 V peak-to-peak voltage (V_{pp}) for the AC signal through experiments. The frequency characteristics of the whole system at the frequency from 3 kHz to 6 GHz are shown in Fig. 2(b). The −3 dB bandwidth of the communication system is 95.34 MHz, which is consistent with the bandwidth of the photodetector. Therefore, the photodetector is the crucial factor restricting the bandwidth of the whole communication system. According to Fig. 2(b), it is found that the system hardly transmits a high-frequency signal of several gigahertz (GHz) through direct detection.

To describe the transmission performance of the system, we introduce the concept of PL, which is defined as[35]

$$\mathrm{PL} = 10 \times \log\left(\frac{P_t}{P_r}\right), \tag{3}$$

where P_t represents the transmitting optical power, and P_r stands for the receiving optical power. On–off keying (OOK) was chosen as a comparison to further highlight the advantages of TGI. The maximum error-free transmission frequencies with varying PL are shown in Fig. 3(a). For OOK, the maximum transmission frequency is 482 MHz without PL, and then it reduces to 200 MHz as the corresponding PL increases to 12.79 dB. For TGI, when PL is below 14.87 dB, it is always capable of maintaining the 4 GHz transmission frequency. After that, the maximum transmission frequency gradually decreases to 400 MHz as PL increases to 18.75 dB. The maximum error-free transmission frequency of TGI is nearly one order of magnitude higher than that of OOK when PL is less than 15 dB. Therefore, the UV-C communication system based on TGI successfully realized the transmission of the high-frequency signals beyond the system bandwidth. This performance is rooted in the principle of the TGI algorithm. In Ref. [36], Chen *et al.* verified this principle further through experiments. Hence, the hardware bandwidth limitation is effectively weakened.

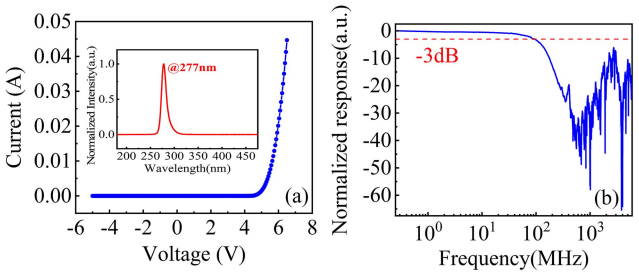

Fig. 2. (a) *I-V* characteristics of UV-C LED. Inset is the normalized spectrum of UV-C LED. (b) Frequency characteristics of the whole system at the optimum operating point.

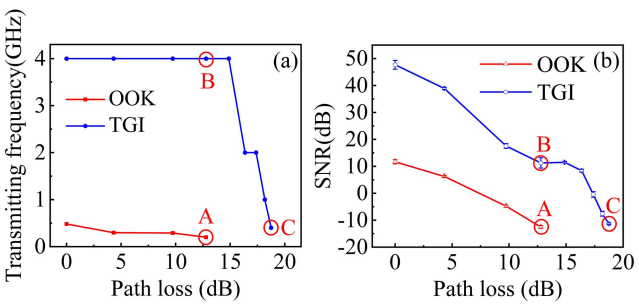

Fig. 3. (a) Comparison of transmitting frequency between OOK and TGI. (b) The calculated SNRs of OOK and TGI. Three points A, B, and C in (a) correspond to (b).

To quantitatively analyze the reason why the TGI curve drops, we calculate the SNRs of the received signals in Fig. 3(a). In general, SNR is defined as

$$\begin{aligned}\mathrm{SNR} &= 10 \times \log \frac{P_{s/n} - P_n}{P_n} \\ &= 10 \times \log \frac{(T_{\mathrm{test}} - \langle T_{\mathrm{test}} \rangle)^2 - (N_{\mathrm{test}} - \langle N_{\mathrm{test}} \rangle)^2}{(N_{\mathrm{test}} - \langle N_{\mathrm{test}} \rangle)^2},\end{aligned} \tag{4}$$

where $P_{s/n}$ and P_n stand for signal power with noise and background noise power, respectively, and T_{test} and N_{test} represent the tested signal amplitude with noise and tested noise, respectively. The calculated results are shown in Fig. 3(b). The SNR of TGI is 47.70 dB (PL = 0 dB), which gradually decreases with the increase of PL and drops to −11.33 dB at point C. Therefore, when PL is higher than 15 dB, the obvious decrease of SNR results in the decrease of the maximum error-free transmission frequency. When PL is less than 15 dB, the SNR remains large even though it decreases, so it has no obvious influence on transmission frequency.

In a word, although high-frequency signal waveforms are severely attenuated due to a lack of bandwidth, the relative amplitude between the original bits is still not significantly affected, so high-frequency signal transmission of GHz can be successfully achieved. However, when the background noise intensity is constant, the SNR at the receiving end is impacted by the dual effects of power attenuation caused by PL and waveform distortion caused by bandwidth limitation. When the attenuation and distortion are severe, the sum of information can no longer be distinguished from the background noise, and the error-free transmission cannot be realized. Therefore, when the SNR is extremely low, the error-free transmission frequency is reduced.

Moreover, the eye diagrams of the A-B-C points in Fig. 3(a) are shown in Figs. 4(a)–4(c), respectively. Comparing Fig. 4(a) with Fig. 4(b), the maximum signal distortion at the sampling instant in the eye diagram of TGI is smaller than that of OOK, and the noise margin is higher than that of OOK. Both indicate that transmission based on TGI has much weaker noise and less intersymbol interference. When the PL is the same, the influence on SNR mainly comes from the bandwidth limitation,

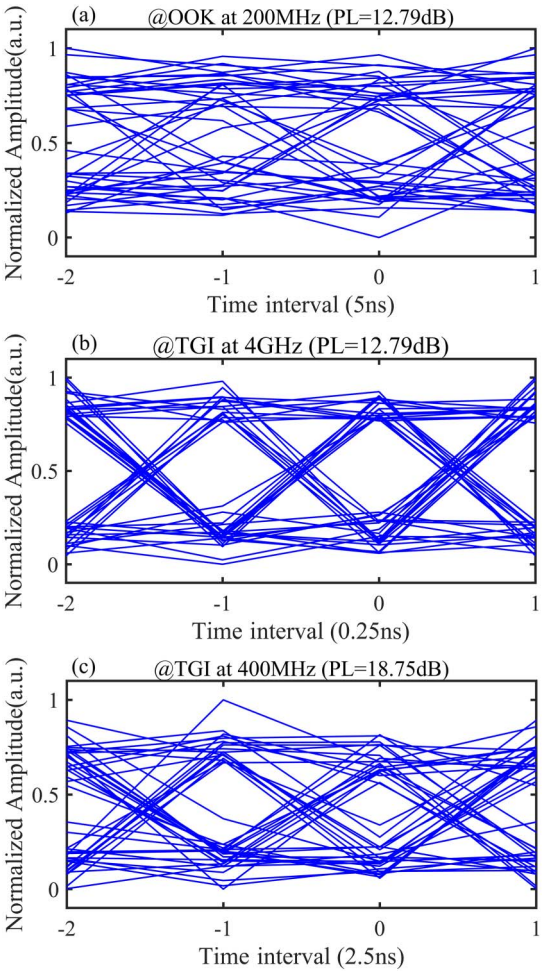

Fig. 4. Eye diagrams comparison among (a) point A, (b) point B, and (c) point C.

so theoretically the eye diagram quality of point B should be worse. On the contrary, the performance of point B is significantly better than that of point A, which effectively proves that the TGI algorithm can optimize SNR. Besides, the difference between these two eye diagrams means that 200 MHz signal transmission through OOK has basically reached the upper limit of the system transmission capacity, while error-free transmission frequency based on the TGI algorithm can be further improved when the PL value is lower than 12.79 dB (point B). Comparing Fig. 4(b) with Fig. 4(c), with the increase of PL, the quality of the eye diagram decreases obviously. Different from the case when the PL value is less than 12.79 dB, the maximum error-free transmission frequency cannot be further increased because of the reduced SNR in the curve descending stage. Comparing Fig. 4(a) with Fig. 4(c), transmission frequency and PL of TGI are both larger than those of OOK, which means that the SNR of TGI is worse than that of OOK. Nevertheless, the eye diagram of TGI still looks cleaner and more regular than that of OOK, which confirms that the TGI algorithm can optimize SNR again. The above analysis of eye diagrams is consistent with that of the calculated SNRs of TGI, which are significantly higher than that of OOK in Fig. 3(b).

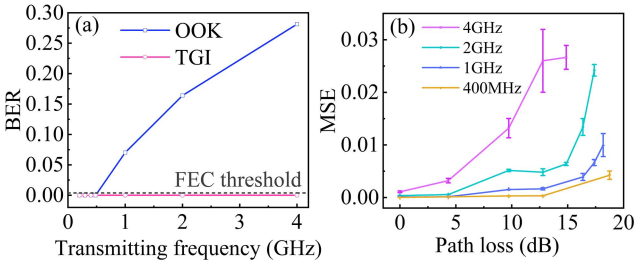

Fig. 5. (a) BER comparison of OOK and TGI (PL = 0 dB). (b) The MSE of TGI at different transmitting frequencies.

The above results show that TGI can weaken the impact of bandwidth limitation to realize high-frequency signal transmission with a low-bandwidth system and simultaneously can effectively improve SNR. These advantages signify that TGI is a potential method to be applied in the field of UV-C communication with low SNR.

Besides, the quantitative analysis for transmission performance under different transmitting frequencies is also necessary. In Fig. 5(a), TGI enables error-free transmission at all frequencies. For OOK, the BER is higher than the forward error correction (FEC) threshold (3.8×10^{-3}) when the frequency is higher than 400 MHz, and BER increases as the frequency increases. This again indicates that the transmission frequency of TGI is much higher than that of OOK. Mean square error (MSE) is introduced to further elaborate the performance of TGI, which is described as[29]

$$\mathrm{MSE} = \sum_{i=1}^{N} [T'(t) - T(t)]^2, \tag{5}$$

where N is the signal length, $T'(t)$ represents the normalized reconstructed signal, and $T(t)$ means the original signal. The smaller the MSE is, the closer the reconstructed signal is to the original signal, and the better retrieved the signal is. The MSE of TGI error-free transmission with changing PL at different transmission frequencies is shown in Fig. 5(b). It is found that PL has a more significant influence on the transmission of the high-frequency signal, which is manifested when the slope of the curve gradually increases with the increase of transmission frequency. In essence, the factor that affects the quality of signal transmission and demodulation is SNR. Compared with the low-frequency signal, the waveform distortion is more serious during high-frequency transmission, so the PL tolerance of the system will be correspondingly weak. This explains why the high-frequency signal is more susceptible to PL, and this conclusion is also consistent with the aforementioned analysis.

4. Conclusion

In conclusion, we first introduced the TGI algorithm to UV-C communication experimentally and further demonstrated the principles, performance, and potential of it in the field of

UV-C communication. TGI was used in the UV-C LED communication system to successfully transmit a 4 GHz signal whose frequency was nearly 40 times above the system bandwidth, and, simultaneously, this transmitting frequency was nearly an order of magnitude higher than that of OOK under the same circumstances. Moreover, the experimental results also show that TGI can effectively optimize the communication performance by improving the SNR. Our research lays a foundation for the application of the TGI algorithm in the UV communication domain and also provides a reference for its prolonged application in other optical communication fields.

Acknowledgement

This work was supported by the National Natural Science Foundation of China (NSFC) (Nos. 61974031 and 61705041), Fudan University-CIOMP Joint Fund (No. FC2020-001), and Shanghai Technical Standard Program (No. 18DZ2206000).

References

1. C. H. Kang, I. Dursun, G. Liu, L. Sinatra, X. Sun, M. Kong, J. Pan, P. Maity, E.-N. Ooi, T. K. Ng, O. F. Mohammed, O. M. Bakr, and B. S. Ooi, "High-speed colour-converting photodetector with all-inorganic $CsPbBr_3$ perovskite nanocrystals for ultraviolet light communication," Light: Sci. Appl. **8**, 94 (2019).
2. G. Chen, Z. Xu, H. Ding, and B. M. Sadler, "Path loss modeling and performance trade-off study for short-range non-line-of-sight ultraviolet communications," Opt. Express **17**, 3929 (2009).
3. X. He, E. Xie, M. S. Islim, A. A. Purwita, J. J. D. McKendry, E. Gu, H. Haas, and M. D. Dawson, "1 Gbps free-space deep-ultraviolet communications based on III-nitride micro-LEDs emitting at 262 nm," Photon. Res. **7**, B41 (2019).
4. Y. Tang, G. Q. Ni, Z. L. Wu, L. J. Zhang, and Y. Lin, "Research on channel character of solar blind UV communication," Proc. SPIE **6829**, 682907 (2007).
5. M. A. El-Shimy and S. Hranilovic, "Spatial-diversity imaging receivers for non-line-of-sight solar-blind UV communications," J. Lightwave Technol. **33**, 2246 (2015).
6. D. Han, Y. Liu, K. Zhang, P. Luo, and M. Zhang, "Theoretical and experimental research on diversity reception technology in NLOS UV communication system," Opt. Express **20**, 15833 (2012).
7. T. Shan, J. Ma, T. Wu, Z. Shen, and P. Su, "Single scattering turbulence model based on the division of effective scattering volume for ultraviolet communication," Chin. Opt. Lett. **18**, 120602 (2020).
8. X. Zhou, X. Tan, Y. Wang, X. Song, T. Han, J. Li, W. Lu, G. Gu, S. Liang, Y. Lü, and Z. Feng, "High-performance 4H-SiC p-i-n ultraviolet avalanche photodiodes with large active area," Chin. Opt. Lett. **17**, 090401 (2019).
9. Z. Xu and B. M. Sadler, "Ultraviolet communications: potential and state-of-the-art," IEEE Commun. Mag. **46**, 67 (2008).
10. S. Karp, R. M. Gagliardi, S. E. Moran, and L. B. Stotts, *Optical Channels* (Springer, 1988).
11. G. A. Shaw, A. M. Siegel, and J. Model, "Extending the range and performance of non-line-of-sight ultraviolet communication links," Proc. SPIE **6231**, 62310C (2006).
12. A. K. Majumdar, Q. He, C. C. Davis, B. M. Sadler, and Z. Xu, "Modulation and coding tradeoffs for non-line-of-sight ultraviolet communications," Proc. SPIE **7464**, 74640H (2009).
13. D.-Y. Peng, J. Shi, G.-H. Peng, S.-L. Xiao, S.-H. Xu, S. Wang, and F. Liu, "An ultraviolet laser communication system using frequency-shift keying modulation scheme," Optoelectron. Lett. **11**, 65 (2015).
14. P. Luo, M. Zhang, D. Han, and Q. Li, "Performance analysis of short-range NLOS UV communication system using Monte Carlo simulation based on measured channel parameters," Opt. Express **20**, 23489 (2012).
15. M. Noshad, M. Brandt-Pearce, and S. G. Wilson, "NLOS UV communications using M-ary spectral-amplitude-coding," IEEE Trans. Commun. **61**, 1544 (2013).
16. C. Xu and H. Zhang, "Packet error rate analysis of IM/DD systems for ultraviolet scattering communications," in *IEEE Military Communications Conference* (2015).
17. Y. Wang and S. Gu, "Ultraviolet communication system based on BPSK subcarrier intensity modulation," Proc. SPIE **9446**, 94461K (2015).
18. https://www.acgih.org/science/tlv-bei-guidelines/.
19. O. Alkhazragi, F. Hu, P. Zou, Y. Ha, C. H. Kang, Y. Mao, T. K. Ng, N. Chi, and B. S. Ooi, "Gbit/s ultraviolet-C diffuse-line-of-sight communication based on probabilistically shaped DMT and diversity reception," Opt. Express **28**, 9111 (2020).
20. H. Qin, Y. Zuo, D. Zhang, Y. Li, and J. Wu, "Received response based heuristic LDPC code for short-range non-line-of-sight ultraviolet communication," Opt. Express **25**, 5018 (2017).
21. H. Qin, Y. Zuo, F. Li, R. Cong, L. Meng, and J. Wu, "Noncoplanar geometry for mobile NLOS MIMO ultraviolet communication with linear complexity signal detection," IEEE Photon. J. **9**, 7906012 (2017).
22. L. Guo, D. Meng, K. Liu, X. Mu, W. Feng, and D. Han, "Experimental research on the MRC diversity reception algorithm for UV communication," Appl. Opt. **54**, 5050 (2015).
23. K. Kojima, Y. Yoshida, M. Shiraiwa, Y. Awaji, A. Kanno, N. Yamamoto, and S. Chichibu, "1.6-Gbps LED-based ultraviolet communication at 280 nm in direct sunlight," in *2018 European Conference on Optical Communication (ECOC)* (2018).
24. H. Yin, H. Jia, H. Zhang, X. Wang, S. Chang, and J. Yang, "Extending the data rate of non-line-of-sight UV communication with polarization modulation," Proc. SPIE **8540**, 85400I (2012).
25. E. Xie, M. Stonehouse, R. Ferreira, J. J. D. McKendry, J. Herrnsdorf, X. He, S. Rajbhandari, H. Chun, A. V. N. Jalajakumari, O. Almer, G. Faulkner, I. M. Watson, E. Gu, R. Henderson, D. O'Brien, and M. D. Dawson, "Design, fabrication, and application of GaN-based micro-LED arrays with individual addressing by N-electrodes," IEEE Photon. J. **9**, 7907811 (2017).
26. https://www.manualslib.com/products/Thorlabs-Apd430a2-10525316.html.
27. B. Sun, M. P. Edgar, R. Bowman, L. E. Vittert, S. Welsh, A. Bowman, and M. J. Padgett, "3D computational imaging with single-pixel detectors," Science **340**, 844 (2013).
28. F. Devaux, P.-A. Moreau, S. Denis, and E. Lantz, "Computational temporal ghost imaging," Optica **3**, 698 (2016).
29. Y.-K. Xu, S.-H. Sun, W.-T. Liu, G.-Z. Tang, J.-Y. Liu, and P.-X. Chen, "Detecting fast signals beyond bandwidth of detectors based on computational temporal ghost imaging," Opt. Express **26**, 99 (2018).
30. W. Meng, D. Shi, K. Yuan, L. Zha, J. Huang, Y. Wang, and C. Fan, "Fourier-temporal ghost imaging," Opt. Lasers Eng. **134**, 106294 (2020).
31. Y. Wang, H. Chen, W. Jiang, X. Li, X. Chen, X. Meng, P. Tian, and B. Sun, "Optical encryption for visible light communication based on temporal ghost imaging with a micro-LED," Opt. Lasers Eng. **134**, 106290 (2020).
32. Y. Tian, H. Ge, X.-J. Zhang, X.-Y. Xu, M.-H. Lu, Y. Jing, and Y.-F. Chen, "Acoustic ghost imaging in the time domain," Phys. Rev. Appl. **13**, 064044 (2020).
33. P. Ryczkowski, M. Barbier, A. T. Friberg, J. M. Dudley, and G. Genty, "Ghost imaging in the time domain," Nat. Photon. **10**, 167 (2016).
34. C. Zhang, S. Guo, J. Cao, J. Guan, and F. Gao, "Object reconstitution using pseudo-inverse for ghost imaging," Opt. Express **22**, 30063 (2014).
35. X. Sun, W. Cai, O. Alkhazragi, E.-N. Ooi, H. He, A. Chaaban, C. Shen, M. H. Oubei, M. Z. M. Khan, T. K. Ng, M.-S. Alouini, and B. S. Ooi, "375-nm ultraviolet-laser based non-line-of-sight underwater optical communication," Opt. Express **26**, 12870 (2018).
36. X. Chen, M. Jin, H. Chen, Y. Wang, P. Qiu, X. Cui, B. Sun, and P. Tian, "Computational temporal ghost imaging for long-distance underwater wireless optical communication," Opt. Lett. **46**, 1938 (2021).